2D AND 3D DEFORMABLE MODELS WITH NARROW BAND REGION ENERGY

Julien Mille, Romuald Boné, Pascal Makris, Hubert Cardot

Université François Rabelais de Tours, Laboratoire Informatique
64 avenue Jean Portalis, 37200 Tours, France
{julien.mille, romuald.bone, pascal.makris, hubert.cardot}@univ-tours.fr

ABSTRACT

We introduce a narrow band region approach in explicit deformable models for 2D and 3D image segmentation. Embedding a region term into the evolution process, we derive a general formulation which is applied both on a 2D parametric contour and a 3D triangular mesh. Evolution of deformable models is performed by means of energy minimization using the computationally efficient greedy algorithm. The use of a region energy related to the vicinity of the evolving surface overcomes limitations of edge-based active models while remaining time effective. Experiments with segmentation quality assessment are carried out on medical images.

Index Terms— Segmentation, narrow band, region energy, active contour, active surface

1. INTRODUCTION

Since their introduction by Kass *et al.*[1], deformable models have met large success in the computer vision community and found many applications in image segmentation and tracking. They are powerful tools thanks to their geometrical adaptiveness and ability to incorporate prior knowledge. Several implementations of these active models were developed in the past. Explicit deformable models represent the evolving boundary as a set of interconnected control points or vertices. Among these, the original 2D parametric contour and the 3D triangular mesh [2] are straightforward implementations, in which the boundary is deformed by direct modifications of vertices coordinates. Conversely, implicit implementations, based on the level set framework, handle the evolving boundary as the zero level of a hypersurface, defined on the same domain as the image. Level sets are often chosen for their natural handling of topological changes and intuitive extensibility to higher dimensions. In this paper, we deal with explicit active contours and surfaces for 2D and 3D segmentation, respectively.

Deformable models are basically attached to the image by means of a local edge-based energies. However, the increasing use of region energies has proven to overcome the limitations of uniquely gradient-based models, especially when dealing with data sets suffering from noise and lack of contrast. Indeed, many anatomical structures encountered in medical imaging lend themselves to region-based segmentation. Many works have dealt with the use of region-based terms in the evolution of deformable models, whether they were implemented as explicit contours [3] or level sets [4]. The region term is based on global image features and is therefore computed over all pixels inside the contour. For parametric snakes, this implies the use of filling algorithms [3] or precomputation of image integrals [5, 6]. Many work has been done using level sets [4, 7] with known advantage of adaptive topology at the expense of computational cost, especially in 3D [8]. Up to now, few region-based approaches have been developed for 3D explicit segmentation as far as we know. Moreover, explicit models have several advantages over their implicit counterparts, including a more intuitive implementation, thus allowing easier modeling of prior knowledge.

We introduce a region-based term with a formulation that can be both applied to explicit parametric 2D contours and 3D meshes. The region energy is computed over a narrow band in the vicinity of the evolving interface, which overcomes limitations of edge-based active models while remaining time effective. Experiments include a comparison with the fast level set method [9]. We first describe the theoretical framework of our models. Then, we deal with numerical implementation issues, including energy minimization by means of the greedy algorithm [10]. Finally, experiments are made on 2D and 3D MRI data sets, including segmentation quality assessment and discussion about weight tuning.

2. NEW REGION-BASED DEFORMABLE MODELS

The continuous active contour model is a closed curve $\mathbf{C} : \Omega \rightarrow \mathbb{R}^2, s \mapsto (x(s), y(s))$. Segmentation of an object of interest is performed by finding the curve $\mathbf{C}$ minimizing the following energy functional:

$$E(\mathbf{C}) = \omega_c E_c(\mathbf{C}) + \omega_e E_e(\mathbf{C}) + \omega_r E_r(\mathbf{C}) \qquad (1)$$

where E_c, E_e and E_r are respectively the curvature, edge and region energies. Parameters ω_c, ω_e and ω_r are the weights defining the relative significance of the corresponding terms. Since we do not wish to minimize curve length, we limit the internal energy to the curvature term:

$$E_c(\mathbf{C}) = \int_\Omega \left| \frac{\partial^2 \mathbf{C}}{\partial s^2} \right|^2 ds \qquad (2)$$

Omitting the first-order regularization term allows the contour to undergo large variations of its area. However, once discretized as a polygon, the contour needs to be periodically reparameterized to keep control points evenly spaced. In this context, resampling and remeshing techniques are discussed in section 3. The two external terms E_e and E_r are the edge and region energies relating the model to the image data. Fitting the contour to salient boundaries implies to use the gradient norm of image function f.

$$E_e(\mathbf{C}) = -\int_\Omega |\nabla f(\mathbf{C}(s))|\, ds \tag{3}$$

Assuming that the curve is simple, i.e. non-intersecting, let R be the region enclosed by $\mathbf{C}$. Hence, $\mathbf{C}$ is a parameterization of ∂R. The region term usually depends on the image function computed over R (the object) and its complement R^C (the background). On explicit implentations, all pixels inside the region should be considered, by means of some region filling algorithm. To increase computational efficiency and flexibility, we introduce a narrow band region energy. We consider that the contour evolves in order to satisfy a region-based term only in its vicinity, i.e. in an inner and outer band on each side of the curve.

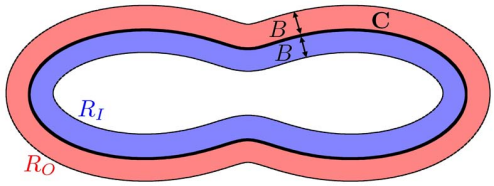

Fig. 1. Inner and outer bands for region energy

Let R_I be the inner band domain and R_O the outer band domain (see fig. 1), and B the band thickness, which is constant as we move along $\mathbf{C}$. The region energy is designed to maximize the mean intensity difference between the inner band and the outer band:

$$E_r(\mathbf{C}) = -\left|\frac{1}{\mathcal{A}_I}\iint_{R_I} f(\mathbf{x})d\mathbf{x} - \frac{1}{\mathcal{A}_O}\iint_{R_O} f(\mathbf{x})d\mathbf{x}\right| \tag{4}$$

where $\mathcal{A}_I$ and $\mathcal{A}_O$ are the band areas. Since the entire regions R and R^C are not considered in the energy functional, they are not forced to verify an intensity homogeneity criterion. Homogeneity is usually not desirable for the backgound in real images. For the object, we should point out that the region energy is used to overcome issues raised by noise and weak edges, rather than seeking for a real region-based partition. To allow easy implementation, integrals of f over regions need to be simplified to line integrals over the contour. Let $\vec{\mathbf{n}}$ be the inward normal defined at every curve point. Region R_I is bounded by $\mathbf{C}$ and $\mathbf{C} + B\vec{\mathbf{n}}$, whereas R_O is bounded by $\mathbf{C}$ and $\mathbf{C} - B\vec{\mathbf{n}}$. We assume that $\mathbf{C}$ is regular enough so that $\mathbf{C} + B\vec{\mathbf{n}}$ and $\mathbf{C} - B\vec{\mathbf{n}}$ are simple curves as well. Let us write our main simplification:

$$\iint_{R_I} f(\mathbf{x})d\mathbf{x} \approx \int_0^B \int_\Omega f(\mathbf{C}+b\vec{\mathbf{n}}) \left|\frac{d(\mathbf{C}+b\vec{\mathbf{n}})}{ds}\right| ds\, db \tag{5}$$

and similarly for R_O, replacing $\vec{\mathbf{n}}$ by $-\vec{\mathbf{n}}$. Rigorously, the line integral of f over $\mathbf{C}$ is:

$$\int_\Omega f(\mathbf{C}(s)) \left|\frac{d\mathbf{C}}{ds}\right| ds \tag{6}$$

where $|d\mathbf{C}/ds|$ is the arc length element. In parametric snakes, it is usually considered constant for the edge energy (conversely, it is considered in geodesic active contours). Removing the arc length makes external energies dependent of the parameterization but makes numerical energy minimization easier.

This approach naturally extends to a three dimensonal segmentation problem. In a continuous space, a deformable model is represented by a parameterized surface $\mathbf{S} : \Omega^2 \to \mathbb{R}^3, (u, v) \mapsto (x(u, v), y(u, v), z(u, v))^T$. Replacing $\mathbf{C}$ by $\mathbf{S}$ in eq. 1, we obtain the surface energy to be minimized. The curvature energy is based on the work in [11], from which we removed the first-order surface derivatives (for the same reason as previously).

$$E_c(\mathbf{S}) = \iint_{\Omega^2} \left|\frac{\partial^2\mathbf{S}}{\partial u^2}\right|^2 + \left|\frac{\partial^2\mathbf{S}}{\partial v^2}\right|^2 du\, dv \tag{7}$$

To compensate the absence of first-order regularization term, the surface will be periodically reparameterized. The edge term $E_e(\mathbf{S})$ may be written as in eq. 3, considering now that f is a $\mathbb{R}^3 \to \mathbb{R}$ function. In the 3D case, the narrow band region energy is computed over the two bands volume integrals.

$$E_r(\mathbf{S}) = -\left|\frac{1}{\mathcal{V}_I}\iiint_{R_I} f(\mathbf{x})d\mathbf{x} - \frac{1}{\mathcal{V}_O}\iiint_{R_O} f(\mathbf{x})d\mathbf{x}\right| \tag{8}$$

where $\mathcal{V}_I$ and $\mathcal{V}_O$ are the band volumes. For instance, should $\mathbf{S}$ be a sphere, R_I and R_O may be viewed as two empty balls with thickness B.

$$\begin{aligned}&\iiint_{R_I} f(\mathbf{x})d\mathbf{x}\\ &\approx \int_0^B \iint_{\Omega^2} f(\mathbf{S}+b\vec{\mathbf{n}}) \left|\frac{d(\mathbf{S}+b\vec{\mathbf{n}})}{du} \times \frac{d(\mathbf{S}+b\vec{\mathbf{n}})}{dv}\right| du\, dv\, db\end{aligned} \tag{9}$$

and similarly for R_O. In last equation, the term between $|.|$ is the area element. As it was done previously in the 2D case, it will be considered as a constant for implementation.

3. IMPLEMENTATION

The contour and surface models are respectively implemented with a polygon and a triangular mesh. Both are described using a common framework. They are made up of a set of n vertices, denoted $\mathbf{p}_i = (x_i, y_i)^T$ in 2D and $\mathbf{p}_i = (x_i, y_i, z_i)^T$ in 3D. Each vertex $\mathbf{p}_i$ has a set of neighboring vertices, denoted N_i. In the 2D contour, index i is the discrete equivalent of the curve parameter, hence $N_i = \{i-1, i+1\}$ ($i+1$ and $i-1$ are modulo n). A vertex has an inward unit normal vector $\vec{\mathbf{n}}_i$. Since the iterative evolution algorithm described below modifies vertex coordinates, all normals should be updated after each iteration (when all vertices have been trans-

lated). To maintain vertices evenly spaced, adaptive resampling (or remeshing in 3D) is performed. The contour and surface are allowed to add or merge vertices to keep the distance between neighboring vertices homogeneous. It ensures that every couple of neighbors $(\mathbf{p}_i, \mathbf{p}_j)$ satisfies the constraint $a \leq |\mathbf{p}_i - \mathbf{p}_j| \leq 2a$, where a is the chosen inter-vertex average distance. Resampling the 2D contour is straightforward, since vertices can be easily inserted at a given position in the vertex list. For the 3D mesh, adding or merging vertices modifies local topology, resulting in triangle merging or splitting [2], as shown in fig. 2.

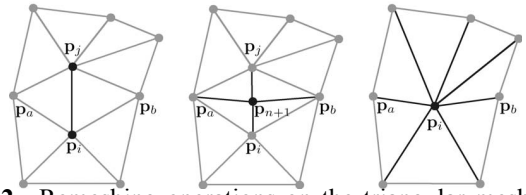

Fig. 2. Remeshing operations on the triangular mesh: initial mesh (left), vertex inserting (middle) and vertex deleting (right)

To minimize the energy functional, the contour or surface is iteratively deformed using the greedy algorithm [12], which was proven to be more efficient than gradient descent [10]. In order the greedy approach to be applicable, the energy is discretized and expressed as a sum of independent vertex energies.

$$E_{global} = \sum_{i=1}^{n} \omega_c E_c(\mathbf{p}_i) + \omega_e E_e(\mathbf{p}_i) + \omega_r E_r(\mathbf{p}_i) + \omega_b E_b(\mathbf{p}_i) \tag{10}$$

For a given vertex $\mathbf{p}_i$, the energy is computed for each $\tilde{\mathbf{p}}_i$ in a square or cubic window around $\mathbf{p}_i$. Let a be the window width and d the image dimension, we have $\tilde{\mathbf{p}}_i \in \{\mathbf{p}_i + \mathbf{r} | \mathbf{r} \in ([-a/2, a/2] \cap \mathbb{Z})^d\}$. Given this, the evolution equation is:

$$\mathbf{p}_i^{(t+1)} = \arg\min_{\tilde{\mathbf{p}}_i} E(\tilde{\mathbf{p}}_i^{(t)}) \tag{11}$$

The internal energy is an approximation of local curvature. While its discretization is simple in 2D, it is not obvious how to implement the surface derivatives of eq. 7 in a triangular mesh. For a discrete planar contour, curvature is equivalent to the squared distance between the vertex and the middle of its two neighbors. Extending this principle to the mesh, the curvature of the tested point $\mathbf{p}'_i$ is the squared distance between $\mathbf{p}'_i$ and the centroid of the neighbors of vertex $\mathbf{p}_i$.

$$E_c(\tilde{\mathbf{p}}_i) = \left| \tilde{\mathbf{p}}_i - \frac{1}{|N_i|} \sum_{j \in N_i} \mathbf{p}_j \right|^2 \tag{12}$$

The edge term $E_e(\tilde{\mathbf{p}}_i) = -|\nabla f(\tilde{\mathbf{p}}_i)|$ is extracted using Sobel and Zucker-Hummel operators for 2D and 3D images, respectively. Gaussian filtering may be applied for noise reduction prior to edge detection. The region energy is a discretization of eq. 4 or 8 depending on the dimension.

$$E_r(\tilde{\mathbf{p}}) = -\left| \sum_{b=0}^{B-1} f(\tilde{\mathbf{p}}_i + b\vec{\mathbf{n}}_i) - \sum_{b=1}^{B} f(\tilde{\mathbf{p}}_i - b\vec{\mathbf{n}}_i) \right| \tag{13}$$

For a given vertex, the same number of voxels is considered in both bands, which allows to avoid normalization by respective areas. It should be noticed that the region term does not use region filling algorithm based polygon scan-conversion, like in [3], thus ensuring lower computational cost. To increase the capture range and to reduce the internal energy shrinking effect, we add a balloon energy E_b derived from the inflation force proposed in [11], which makes the model propagate along its normal direction.

$$E_b(\tilde{\mathbf{p}}_i) = |\tilde{\mathbf{p}}_i - (\mathbf{p}_i + a\vec{\mathbf{n}}_i)|^2 \tag{14}$$

The sign of weight ω_b appearing in eq. 10 controls the motion orientation, whether the balloon is used to inflate or deflate the surface.

4. RESULTS

Segmentation experiments were conducted on real medical data on a P4 2.8GHz with 512Mb RAM. Expert segmentation was available, so that segmentation quality can be assessed. The modified Hausdorff distance $\mathcal{H}_{mean}$ introduced in [13] measures the average fitting of the surface to the real boundary, whereas the original Haussdorf distance $\mathcal{H}_{max}$ corresponds to the greatest error between the two boundaries. Both are expressed in pixel/voxel units.

We compared our method to the Chan & Vese model [4] implemented using the fast evolution algorithm described in [9]. We consider the level set function $\phi : \mathbb{R}^d \rightarrow \mathbb{R}$, where d is the image dimension. The contour or surface is the zero level set of ϕ. We define the region enclosed by the contour or surface by $R = \{\mathbf{x} | \phi(\mathbf{x}) \geq 0\}$. Function ϕ deforms according to the evolution equation:

$$\frac{\partial \phi}{\partial t} = F(\mathbf{x}) \left| \nabla \phi(\mathbf{x}) \right| \ \forall \mathbf{x} \in \mathbb{R}^d \tag{15}$$

with speed function F defined as follows:

$$\begin{array}{rcl} F(\mathbf{x}) & = & F_e(\mathbf{x}) + F_r(\mathbf{x}) - \kappa(\mathbf{x}) \\ F_e(\mathbf{x}) & = & -\left| \nabla f(\mathbf{x}) \right| \\ F_r(\mathbf{x}) & = & -\left| \mu_I - f(\mathbf{x}) \right| + \left| \mu_O - f(\mathbf{x}) \right| \\ \kappa(\mathbf{x}) & = & \mathrm{div}(\nabla \phi / \left| \nabla \phi \right|) \end{array} \tag{16}$$

where κ is the curvature of ϕ. μ_I and μ_O are the mean intensities inside and outside the contour. F_e and F_r are the edge and region terms.

Typically, classical edge-based deformable models fail on medical data, where noise and low contrast prevent the extraction of reliable boundaries. Fig. 3 depicts segmentation of the left ventricle, in a 256×256 MRI slice in short-axis view. The main application here is the measurement of blood volumes to estimate the ejection fraction, a critical value in cardiac disease diagnosis. Finding the endocardium boundary is made more complex by the presence of papillary muscles, appearing as small dark areas inside the blood pool. For this particular data, topological changes were handled. The need for a topological modification was detected by verifying intersection between at least two contour edges. We used region filling and edge linking algorithms to compute the new set of

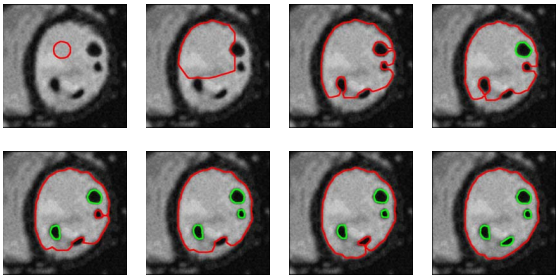

Fig. 3. Segmentation of the left ventricle endocardium: topological changes generate small inner boundaries (green) inside the main boundary (red)

contours. When the active contour wrapped around a papillary muscle, an independent deformable contour was created. Our approach proved to be robust with respect to initial location as long as the major part was inside the blood pool. Obtained distance values were $\mathcal{H}_{mean} = 0.54$ and $\mathcal{H}_{max} = 2.32$ with our method and $\mathcal{H}_{mean} = 0.68$ and $\mathcal{H}_{max} = 2.78$ for the level set method. We found our method to be slightly slower than the level set (about $3s$), mainly due to topological handling. Figure 4 shows a reconstructed surface of the aorta, in a 3D $512 \times 512 \times 810$ CT data set of the abdomen. A fixed-topology 3D mesh was initialized as a sphere totally inside the blood vessel and inflated afterwards. Measurement of the final surface with respect to ground truth gave ($\mathcal{H}_{mean} = 1.07$, $\mathcal{H}_{max} = 13.37$) for our method, whereas we obtained ($\mathcal{H}_{mean} > 20$, $\mathcal{H}_{max} > 20$) with the implicit surface method. Indeed, level sets have difficulties to generate boundaries as smooth as explicit surfaces do, which is maily due to their implicit curvature. Even with stronger curvature weight, the implicit surface was subject to boundary leakages. We found that band thickness B was not critical above 5 voxels on final quality, but was the major influence on computational cost. Full segmentation process took $84s$ with $B = 10$ and $62s$ with $B = 5$, whereas the fast level set took more than $300s$ to reach the same segmentation level.

5. CONCLUSION

We proposed a new narrow band region term for explicit deformable models driven by energy minimization. Our approach is based on a general formulation allowing implementation on discrete 2D active contours and 3D triangular meshes. The narrow band region energy managed to overcome the drawbacks of gradient-based models with very promising results, in terms of computational cost and segmentation quality. Future work may focus on handling topological modifications on the mesh, like in [2]. We also plan to extend the model for region tracking on 3D temporal data, and investigate further on the criteria for comparisons between explicit approaches and level set methods.

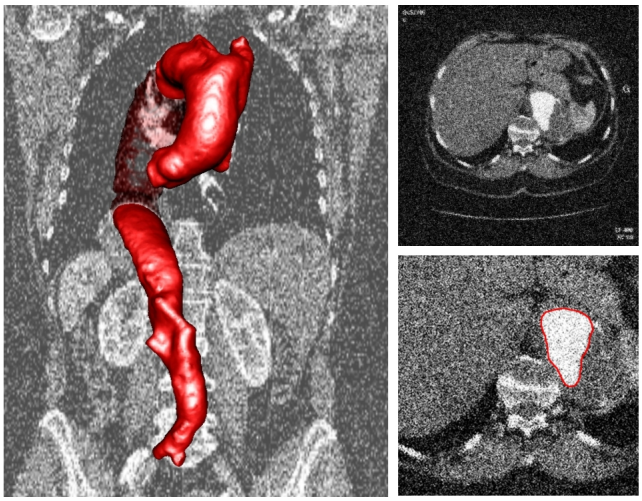

Fig. 4. Segmented aorta in abdominal CT: 3D surface (left), single slice (top-right) and segmented slice with scale $\times 2$ (bottom-right)

6. REFERENCES

[1] M. Kass, A. Witkin, and D. Terzopoulos, "Snakes: active contour models," *International Journal of Computer Vision*, vol. 1, no. 4, pp. 321–331, 1988.

[2] J.O. Lachaud and A. Montanvert, "Deformable meshes with automated topology changes for coarse-to-fine three-dimensional surface extraction," *Medical Image Analysis*, vol. 3, no. 2, pp. 187–207, 1999.

[3] J. Ivins and J. Porrill, "Active region models for segmenting textures and colours," *Image and Vision Computing*, vol. 13, no. 5, pp. 431–438, 1995.

[4] T. Chan and L. Vese, "Active contours without edges," *IEEE Trans. IP*, vol. 10, no. 2, pp. 266–277, 2001.

[5] A. Chakraborty, L. Staib, and J. Duncan, "Deformable boundary finding in medical images by integrating gradient and region information," *IEEE Trans. MI*, vol. 15, no. 6, pp. 859–870, 1996.

[6] M. Jacob, T. Blu, and M. Unser, "Efficient energies and algorithms for parametric snakes," *IEEE Trans. IP*, vol. 13, no. 9, pp. 1231–1244, 2004.

[7] F. Lecellier, S. Jehan-Besson, M.J. Fadili, G. Aubert, M. Revenu, and E. Saloux, "Region-based active contours with noise and shape priors," in *IEEE ICIP*, Atlanta, USA, 2006.

[8] A. Dufour, V. Shinin, S. Tajbakhsh, N. Guillén-Aghion, J.-C. Olivo-Marin, and C. Zimmer, "Segmenting and tracking fluorescent cells in dynamic 3-D microscopy with coupled active surfaces," *IEEE Trans. IP*, vol. 14, no. 9, pp. 1396–1410, 2005.

[9] Y. Shi and W. Karl, "Real-time tracking using level sets," in *IEEE CVPR*, San Diego, USA, 2005, vol. 2, pp. 34–41.

[10] J. Mille, R. Boné, P. Makris, and H. Cardot, "Greedy algorithm and physics-based method for active contours and surfaces: a comparative study," in *IEEE ICIP*, Atlanta, USA, 2006.

[11] L.D. Cohen and I. Cohen, "Finite element methods for active contour models and balloons for 2D et 3D images," *IEEE Trans. PAMI*, vol. 15, no. 11, pp. 1131–1147, 1993.

[12] D.J. Williams and M. Shah, "A fast algorithm for active contours and curvature estimation," *CVGIP: Image Understanding*, vol. 55, no. 1, pp. 14–26, 1992.

[13] M-P. Dubuisson and A.K. Jain, "A modified Hausdorff distance for object matching," in *ICPR*, Jerusalem, Israel, 1994, pp. 566–568.